Master's Thesis

석사 학위논문

Characterization of Interaction between Pathogenic PolyQ Proteins and Q-rich Target Proteins

GYU REE KIM (김 규 리 金 奎 里)

Department of Brain and Cognitive Science

뇌.인지 과학전공

DGIST

2016

Characterization of Interaction between Pathogenic PolyQ Proteins and Q-rich Target Proteins

Advisor: Professor Sung Bae Lee

Co-Advisor: Professor Kee Tae Kim

by

GYU REE KIM
Department of Brain and Cognitive Science
DGIST

A thesis submitted to the faculty of DGIST in partial fulfillment of the requirements for the degree of Master of Science in the Department of Brain and Cognitive Science. The study was conducted in accordance with Code of Research Ethics[1)].

11. 23. 2015

Approved by

Professor Sung Bae Lee _____

(Advisor)

Professor Kee Tae Kim _____

(Co-Advisor)

[1)] Declaration of Ethical Conduct in Research: I, as a graduate student of DGIST, hereby declare that I have not committed any acts that may damage the credibility of my research. These include, but are not limited to: falsification, thesis written by someone else, distortion of research findings or plagiarism. I affirm that my thesis contains honest conclusions based on my own careful research under the guidance of my thesis advisor.

Characterization of Interaction between Pathogenic PolyQ Proteins and Q-rich Target Proteins

GYU REE KIM

Accepted in partial fulfillment of the requirements for the degree of Master of Science.

11. 23. 2015

Head of Committee_____
Prof. Sung Bae Lee

Committee Member_____
Prof. Kyuhyung Kim

Committee Member_____
Prof. Kee Tae Kim

MS/BS 201425003

김 규 리. GYU REE KIM. Department of Brain and Cognitive Science. 2016. Characterization of Interaction Between Pathogenic PolyQ Proteins and Q-rich Target Proteins. 43p. Advisors Prof. Lee, Sung Bae, Co-Advisors Ph.D. Kim, Kee Tae.

Abstract

To understand the pathogenesis of many diseases attributed to protein toxicity such as polyglutamine (polyQ) diseases, it is very crucial to determine how these toxic disease proteins interact and trap their numerous targets. However, in polyQ diseases, details of required features for their interaction with targets remain largely unknown. Here, we identified what features are necessity for interaction between polyQ and targets, and how target proteins have an effect on polyQ aggregate formation. We visualized the interaction between pathogenic polyQ proteins and Q-rich possible target proteins in neurons, which is predicted on the Q-Q based protein interaction occurring in pathogenic polyQ-containing proteins for their self-oligomerization/aggregation. Furthermore, we checked whether the interaction of pathogenic polyQ proteins with targets can be modulated through designed strategies such as using a structural inhibitor molecule. Through this study, we established the model system to study the modes of interaction between pathogenic polyQ and Q-rich target proteins and aim to prove the possibility of target proteins accelerating aggregate formation by acting as glue.

Keywords: Polyglutamine disease, Q-rich proteins, target proteins, interaction, glue theory

List of contents

List of Figures

Figure 2. Identified Q-rich proteins based on the two features of Q-richness

Canonical amino acid sequences of 13,738 proteins deposited in UniProt reference proteome for *Drosophila melanogaster* were collected (Left panel). Calculated the density of glutamine (Q) residues defined as the number of Q residues divided by sequence length (Upper Right). Calculated the number of patches composed of seven or more continuous Q residues (Lower Right). The density of Q residues > 9.0×10^{-2} (95^{th} percentile of the distribution of the density of Q residues for whole proteins)

Figure 3. Co-localization between possible Q-rich target proteins and pathogenic polyQ protein (Huntingtin, Htt)

Images of co-localization between possible Q-rich target proteins (MED25, MED11, Dsp1, nej/CBP) and pathogenic polyQ protein (Htt152Q). (Left) Localization of Q-rich target proteins. (Right) Co-express between pathogenic polyQ protein (Htt152Q) and target proteins (MED11, MED25, Dsp1 and CBP). Arrowheads indicate co-localization.

Figure 4. Overexpressing of target proteins with polyQ protein increase aggregate formation

Figure 4.1 Overexpression of target protein (MJDtr27Q) with pathogenic polyQ protein (Htt152Q) increase aggregate numbers. Arrowhead indicated aggregates.

Figure 4.2 Quantification of aggregate numbers in class IV da neurons expressing denoted transgenes (control (Htt152Q), Htt152Q+MJD27Q). Bars indicate mean ± SD; n = 6; $^{**}P < 0.01$ (Student's unpaired t test) relative to control.

Figure 4.3 Overexpression of target protein (MED11 and MED25) with pathogenic polyQ protein (Htt152Q) increase aggregate numbers. Arrowhead indicated aggregates.

Figure 4.4 Quantification of aggregate numbers in class IV da neurons expressing denoted transgenes (control (Htt152Q), Htt152Q+MED11 and Htt152Q+MED25). Bars

indicate mean ± SD; $n = 6$; ***$P < 0.001$ (Student's unpaired t test) relative to control.

Figure 5. Interaction/aggregate formation between pathogenic polyQ and Q-rich target proteins suppressed by QBP1

Figure 5.1 The proposed schematic diagram for the key implication of our study; (1) Q-rich target proteins interact with pathogenic polyQ proteins (2) by working as glue (increasing interaction property), (3) and possible strategy of preventing interaction opportunity using structural inhibitor, QBP1

Figure 5.2 Localization of CBP in *Drosophlia* da neurons. Pathogenic polyQ (Htt152Q) interacts with CBP in cytoplasm (Upper panel). QBP1 inhibit aggregate formation in da neurons of Htt152Q+CBP (Lower panel). CBP seems to be released from pathogenic polyQ protein (Htt152Q).

Figure 5.3 Quantification of CBP signal intensity in nucleus expressing denoted transgenes (control (Htt152Q+CBP), Htt152Q+CBP+QBP1). Bars indicate mean ± SD; $n = 20$; ***$P < 0.001$ (Student's unpaired t test) relative to control.

Figure 5.4 Quantification of aggregate numbers in da neurons expressing denoted transgenes (control (Htt152Q+CBP), Htt152Q+CBP+QBP1). Bars indicate mean ± SD; $n = 20$; **$P < 0.01$ (Student's unpaired t test) relative to control.

Figure 6. RNA interference of target proteins decreases pathogenic polyQ protein (Htt) aggregate numbers.

Figure 6.1 RNA interference of target protein (MED25 RNAi, MED11 RNAi and Dsp1 RNAi) with pathogenic polyQ protein (Htt152Q) decrease aggregate numbers.

Figure 6.2 Quantification of aggregate numbers in da neurons expressing denoted transgenes (Htt152Q, Htt152Q+MED11 RNAi, Htt152Q+MED25 RNAi, Htt152Q+Dsp1

RNAi). Bars indicate mean ± SD; $n = 12$; ***$P < 0.001$ (Student's unpaired t test) relative to control.

Supplementary figure 1. Localiztion of polyQ proteins (MJD and Htt)

Supplementary figure 1.1 Localization of Ataxin-3 (MJD/SCA3) expressions in da neurons. MJD27 localizes to the cytoplasm (Upper panel) MJD78Q localizes to the nucleus (Lower panel). Dotted lines appear nucleus.

Supplementary figure 1.2 Localization of Huntingtin (Htt) expressions in da neurons. Htt18Q (Upper panel) and Htt152Q (Lower panel) localize to the cytoplasm. Dotted lines appear nucleus.

Supplementary figure 2. Confocal images of nej/CBP expressions with MJD78Q in da neurons. Dotted lines appear nucleus.

Supplementary figure 3. Interaction/aggregate formation between pathogenic polyQ and Q-rich target proteins suppressed by HSPs

Supplementary figure 3.1 The schematic diagram for sequestering or trapping the plausible targets of the polyQ aggregates, and their transition modes from reversible mode to irreversible mode.

Supplementary figure 3.2 Heat shock proteins prevent aggregate formation between pathogenic polyQ and target protein. Co-localiztion of pathogenic polyQ protein (Htt152Q) and Q-rich target protein (nej/CBP) (Upper panel). Co-expressed Hsp70 with Htt152Q + nej/CBP (Middle panel), and Hsp40 with Htt152Q+nej/CBP (Lower panel) in neurons.

Supplementary figure 3.3 Quantification of nej/CBP signal intensity in nucleus expressing denoted transgenes (control (Htt152Q+nej/CBP), Htt152Q+nej/CBP+HSP70,

Htt152Q+nej/CBP+HSP40). Bars indicate mean ± SD; $n = 20$; ***$P < 0.001$ (Student's unpaired *t* test) relative to control.

Supplementary figure 4. Effects of chaperones on pathogenic polyQ protein(Htt152Q).

Supplementary figure 4.1 Confocal images of aggregate formation in neurons. Htt152Q (Upper panel), Htt152Q and Hsp70 (Middle panel) and Htt152Q and Hsp46 (Lower panel). Co-expression of Hsp40 significantly reduced huntingtin aggregation

Supplementary figure 4.2 Quantification of the aggregate formation numbers in neurons expressing denoted transgenes (control (Htt152Q+nej/CBP), Htt152Q+nej/CBP+HSP70, Htt152Q+nej/CBP+HSP40). Bars indicate mean ± SD; $n = 11$; ***$P < 0.001$ (Student's unpaired *t* test) relative to control.

List of tables

I. Introduction

The polyglutamine (polyQ) diseases are representative neurodegenerative diseases that are caused by intracellular accumulation of toxic proteins containing expanded glutamine (CAG) repeats (Zoghbi, H. Y. & Orr, H. T., 2000, Orr, H. T. & Zoghbi, H. Y., 2007). Although polyQ diseases are classified into at least nine subtypes including Huntington's disease (HD) and several types of ataxias depending on the mutated genes responsible for the diseases, they share several common features. Commonly shared prominent feature is self-oligomerization of toxic proteins in either nucleus or cytoplasm of neurons, possibly resulting in neuronal dysfunction. To explain the pathogenesis of polyQ diseases involving toxic protein accumulation inside the cell (Ross, C. A. & Poirier, M. A., 2004, Arrasate, M., 2004), toxicity arisen from sequestration of their numerous target proteins, resulting in their loss of function, can be considered. Seemingly, the formed disease protein complexes trapping targets are the key contributor of disease pathogenesis. Although many studies have been actively done to uncover possible targets of pathogenic polyQ proteins, still detailed mechanisms behind their interaction modes are largely elusive.

To date, many targets of polyQ proteins such as CREB-binding protein (CBP) (McCampbell, A. *et al.* 2000), TATA-binding protein (TBP) and Capicua have been identified. Interestingly, many of these polyQ targets have long patch of Q and high Q content in common. Based on these commonalities, it has been reported that pathogenic

polyQ proteins are expressed by self-oligomerization of expanded polyQ proteins, and interact with various Q-rich proteins. Thus, we assumed Q-Q interaction as the main contributor for polyQ pathogenesis. While many studies have focused on elucidating the mode of pathogenic polyQ self-oligomerization, their interaction mode with other target molecules is still vague. Releasing interaction between Q-rich target proteins and polyQ proteins can provide effective strategy to alleviate toxicity of polyQ proteins. Taken togather, understanding a way of interaction between poly Q proteins and other Q-rich-targeted proteins, and releasing these interactions are indispensable.

Here, we established a good model system for studying the target interaction of pathogenic polyQ proteins. Using this model system, we found that pathogenic polyQ proteins were able to trap/sequester Q-rich proteins, and target proteins are able to accelerate aggregate formation with working as glue. For the future study, we identify what makes them different from other Q-rich proteins able to interact with polyQ proteins will provide deeper insight on the pathogenic mechanism of polyQ proteins.

II. Methods

2.1. Fly stocks

The UAS -*Htt*-18Q-eGFP, UAS-*Htt*-152Q-eGFP, UAS-NLS-*Htt*-18Q, UAS-NLS-*Htt*-152Q fly lines were obtained from A. W. Moore (RIKEN Brain Science Institute, Japan). The *ppk*-gal4, *109(2)80*-gal4, *2-21*-gal4, and UAS-*mCD8GFP* were used as we have previously described (Ye et al., 2004, Lee et al., 2011). The UAS-*MJD-27Q*, UAS-*MJD-78Q*, UAS-*nej-V5*, MED25 RNAi-42501, Dsp1 Ri 31960, MED11 Ri 57815, UAS- velo 44374 and *elav*-gal4 fly lines were obtained from the Bloomington Stock Center. UAS-MED25 F000991, UAS-MED11 F001167, UAS-Dsp1 F000072 gal4 fly lines were obtained from the FlyORF Stock Center. Flies were raised at 25°C.

2.2. Identification of Q-rich proteins

Canonical amino acid sequences of 13,738 proteins deposited in UniProt reference proteome[1] for *Drosophila melanogaster* were collected. Using these sequences, we identified Q-rich proteins based on the two features of Q-richness. For each protein,

we first calculated the density of glutamine (Q) residues defined as the number of Q residues divided by sequence length. We then calculated the number of patches composed of seven or more continuous Q residues. We identified Q-rich Proteins as the ones that have the density of Q residues > 9.0×10^{-2} (95^{th} percentile of the distribution of the density of Q residues for whole proteins) and contain at least one continuous Q patch

1 UniProt, C. UniProt: a hub for protein information. *Nucleic acids research* **43**, D204-212, doi:10.1093/nar/gku989 (2015).

2.3. Immunostaining

Third instar larvae fillet was fixed with 4% formaldehyde (Junsei, Japan) without or with 4% sucrose, respectively, for 20 minutes at room temperature. After rinsed with washing buffer (0.3% Triton X-100 in Phosphate Buffered Saline), samples were treated with blocking buffer (Normal Donkey Serum at a concentration of 1:20 in washing buffer) for an hour at room temperature. Samples were then incubated overnight at 4°C with primary antibodies of rat anti-HA (3F10, Roche Applied Sciences; 1:100 dilution), mouse anti-V5 (R960-25, 1:5,000 dilution), with or without rabbit anti-GFP (1:1,000 dilution) in blocking buffer. After several rinsing with washing buffer for 30 minutes, samples were incubated further with fluorescent dye-conjugated secondary antibodies (Jackson Immunoresearch Laboratories; 1:200 dilution) for 2~4 hours at room temperature. Cy3-conjugated anti-HRP (Jackson

Immunoresearch Laboratories; 1:200 dilution) staining was used together with the secondary antibodies to label membrane of dendrites of whole da neurons in larvae fillet. After washing, samples were mounted with 70% glycerol in phosphate buffered saline (PBG) for imaging.

2.4. Statistical analysis for significant test

Student's unpaired t-test (Microsoft Office Excel's T-TEST) was used for statistical comparison.

2.5. Microscope Imaging

Imaging was carried out by using a ZeissLSM700 and ZeissLSM780 confocal system.

Images were taken with 40x oil lens at the temperature of 21℃. PBG was used as a mounting solution. Images were acquired through a Zen (Zeiss LSM700 and 780) program and processed by Adobe Photoshop program.

III. Result

3.1. Pathogenic polyQ proteins interact with Q-rich polyQ proteins.

Previous study with polyQ disease, ataxin-3 [SCA3 (Spinocerebellar ataxia type 3) / MJD (Machado–Joseph disease)], rescue eye phenotype and generally suppresses degeneration induced by pathogenic polyQ proteins in Drosophila (Warrick et al., 2005). Although such ataxin-3 normal polyQ proteins may contribute to rescue from pathogenesis, we tested mutation forms of ataxin-3 (MJD27Q-FL C14A). It did not rescue and modulate degeneration, but rather accelerate toxicity phenotypically in Drosophila neurons (Figure 1.1 and 1.2).

To investigate what happen to these proteins and how normal polyQ proteins change its subcellular location, we co-expressed of normal ataxin-3 (MJD27Q) and pathogenic form of ataxin-3 (MJD78Q). As a result, we observed that MJD27Q is trapped in MJD78Q (Figure 1.3). We assumed polyQ proteins trap target proteins depending on its contents of glutamines (Q).

To determine whether target proteins can be trapped in pathogenic polyQ proteins, we compared subcellular locations using both normal and expanded Q repeat lengths. MJD and Htt are utilized to modulate Q-contents genetically. Generally, previous studies also showed normal MJD proteins located in cytoplasm, but pathogenic forms located in nucleus. In contrast, huntingtin (Htt) located in cytoplasm both normal and pathogenic conditions (Supplementary Figures 1.1 and 1.2). We observed co-expressed each two types of pathogenic polyQ proteins, Htt152Q and MJD78Q, and normal polyQ proteins, Htt18Q and MJD27Q. As a result, Htt152Q trapped MJD78Q in cytoplasm, but normal polyQ proteins did not interact with each other proteins (Figure 1.4). Next, we examined expression of different subcellular proteins location, using *nuclear-localization-signal* (NLS) -Htt152Q and Htt-152Q with MJD27Q flies. We observed Q-rich proteins were trapped in pathogenic Q-expansion proteins in cytoplasm as well as nucleus (Figure 1.5). It suggested that pathogenic polyQ proteins trapped Q-rich target proteins, regardless of subcellular location and indicated that Q-contents/lengths are important factor between pathogenic polyQ proteins and target proteins interaction.

3.2. Possible target proteins in the cell and Co-localization between possible Q-rich target proteins and pathogenic polyQ protein

According to the results above findings, we assumed that there are numerous Q-rich target proteins, including polyQ proteins and high continuous Q or high Q contents proteins, and those are able to be targets of pathogenic polyQ proteins. Several previous studies (Tait et al., 1998; Orr and Zoghbi, 2007) showed that the pathogenic MJD polyQ protein interacts with the nuclear proteins including the polyQ patch, and/or sequesters transcription factors into their aggregates.

However, there is a limit to figure out the modes of interaction, because they are all polyQ proteins. To generalize our hypothesis, we should have analyzed other cellular proteins. For this, we found canonical amino acid sequences of 13,738 proteins deposited in UniProt reference proteome for *Drosophila melanogaster* were collected (Figure 2.1). Using these sequences, we identified Q-rich proteins based on the two features of Q-richness. For each protein, we first calculated the density of glutamine (Q) residues defined as the number of Q residues divided by sequence length (Figure 2.2). We then calculated the number of patches composed of seven or more continuous Q residues (Figure 2.3). We identified numerous Q-rich proteins existed in the cellular level systematically and it supports that pathogenic polyQ proteins can sequester/trap their potential target proteins.

We next explored whether possible Q-rich target proteins could be trapped in pathogenic polyQ proteins. We used several available fly lines, Mediator Complex Subunit 25 (MED25),

Mediator Complex Subunit 11 (MED11), Dorsal switch protein 1 (Dsp1), Veloren (velo) in the Table1, and CREB (cAMP response element binding) Binding Protein (CBP). CBP is already largely recognized as target proteins trapped in polyQ proteins, the Htt and the MJD (SCA3/Atx-3) in vitro (McCambell et al. 2000; Steffan et al.2001; Nucifora et al. 2001). In addition, we also screened the list of Q-rich proteins in Human by Table. 2.

At first, we showed where the possible target proteins localization in normal condition of neurons (Figure 3.1), then co-expressed with Htt152Q (Figure 3.2). MED11, MED25, DSP1 and CBP are co-localization with Htt152Q, even they have different tendency. However, velo is not co-localized with Htt152Q (data not shown). We assumed that possible target of Q-rich proteins have different own characterization, then those all targets are not able to trap with pathogenic polyQ proteins. Taken together, these results suggest that possible targets of Q-rich proteins exist in the general cellular condition and several possible Q-rich target proteins co-localized with pathogenic polyQ proteins.

3.3. Overexpressed target proteins with polyQ proteins increased aggregation form

To corroborate the above observation, we investigated the sequestration effect of expanded polyQ proteins with interacting partners. For the purpose of confirming the possible involvement of Q-rich target proteins in aggregate formation of polyQ proteins, we tested whether target proteins increase the aggregate formation or not when the target proteins were increased. The result showed that overexpressed target proteins such as MJD-27Q, MED11 and MED25, are able to increase aggregate formation numbers (Figures 4A and 4C). There seemed to be significant in the number of aggregate formations between Htt152Q and MJD-27Q, MED11, and MED25 (Figures 4B and 4C). Particularly, MED25 formed the number of aggregate formations (Figure 4C). These results suggest that Q-rich target proteins in pathogenic polyQ proteins might play an important role in accelerating the interaction between polyQ proteins and targets and their toxicities.

3.4. QBP1 prevent interaction between polyQ proteins and target proteins

We know from previous experiment that overexpressed target proteins are able to increase aggregate forms in pathogenic polyQ proteins by acting as glue. To define the Q-rich target proteins really work as glue for accelerating polyQ aggregate formation, we used the peptide inhibitor for preventing interaction between pathogenic polyQ proteins and Q-rich target proteins. Thus, we used Q-Binding Protein 1 (QBP1) which is designed to obstruct specifically binding to the expanded polyQ stretch and inhibits neurodegeneration in Drosophila models of the polyQ diseases. It can also prevent the misfolding/aggregation of proteins (Popiel HA et al. 2007, Popiel HA et al. 2011, Popiel HA et al. 2013).

Therefore, we designed the model strategies on the supposition that the possibility of Q-Q based interaction. First one is interaction between polyQ disease and target protein, and second one is about in case of increased Q-rich target proteins pool, resulting in accelerating aggregate formation (Figures 5.1-1, -2). The last one showed feasibility of preventing their interaction using QBP1 (Figure 5.1-3). Based on hypothesis, we tested whether QBP1 prevent interaction between pathogenic polyQ (Htt152Q) and its target protein. Interestingly, CBP seemed likely that it could be released from Htt152Q through function of QBP1 (Figure 5.2). CBP signal intensity in nucleus significantly increased (Figure 5.3) and aggregate formations also alleviated (Figure 5.4). It suggested that QBP1 plays a role in inhibiting interaction between pathogenic polyQ protein and Q-rich target protein as a shield, and it is also able to decrease aggregate formations, resulting from their interactions.

In addition, we used Heat Shock Proteins (HSPs) the other strategy for alleviating interaction between pathogenic polyQ proteins and target proteins. In the previous studies, they show that several chaperons, including Hsp40, Hsp70, and N-ethylmaleimide-sensitive factor (NSF), can inhibit cellular toxicity caused by N-terminal mutant huntingtin fragments (Zhou, H. et al. 2001, Muchowski, P. J. et al, 2000, Wyttenbach, A. et al. 2000, Chai, Y. et al. 1999). Also, we assumed that there are transition modes of Q-Q based interaction between polyQ proteins and target proteins, reversible stage and irreversible stage (Supplementary figure 3.1). We suggested that QBP1 works in reversible stage, because it was not enough to alleviate aggregation numbers (Supplementary figure 3.1). We expected better result to decrease aggregate formation using HSPs at the irreversible stage based on the main function of chaperones. At first, we tested HSPs to pathogenic polyQ protein (Htt152Q) only (Supplementary figure 4.1) and the average number of aggregation significantly decrease between Htt152Q and nej/CBP (Supplementary figure 4.2). Then, we showed effect of Hsp40 and Hsp70 in the interaction between pathogenic polyQ protein (Htt152Q) and target protein (nej/CBP) (Supplementary figure 3.2), nej/CBP signal intensity increase in nucleus by Hsp40 (Supplementary figure 3.3). These data supported that molecular chaperones may act essentially by channeling toxic protein into nontoxic aggregates, thus preventing or delaying disease initiation and perhaps slowing disease progression.

3.5. RNA interference of target proteins decreased polyQ protein (Htt) aggregate numbers

To confirm our hypothesis, we experimented whether Htt aggregate numbers decrease using gene silencing approaches specifically RNA interference (RNAi). RNAi downregulate gene expression by including enzyme-dependent degradation of targeted mRNA (Kole R et al. 2012). We expected that target proteins RNAi approaches would be predicted to reduce opportunities of interaction between pathogenic polyQ and target proteins and decrease aggregate formation numbers including toxicity by regulating transcription levels of genes.

For the purpose of confirming the possible involvement of target proteins in aggregates formation of proteins, we tested co-expressed target proteins RNAi, MED25 RNAi, MED11 RNAi and Dsp1 RNAi with Htt152Q (Figure. 6). As a result, surprisingly, aggregate formation numbers are significantly reduced in neurons, depending upon different kind of target proteins. It supports that the pathogenic polyQ protein traps/sequesters Q-rich target proteins, and target proteins expression level also plays an important role in accelerating aggregate formations. To sum up, it is very likely that the pathogenic polyQ protein directly or indirectly interact with Q-rich target proteins, and Q-rich target proteins are working as a glue in Q-Q based interaction.

I. DISCUSSION

Despite of many previous studies on the polyQ diseases, still our understanding on the molecular details of the targets such as required features to be a polyQ protein target remains elusive. Here, in this study, we have identified Q-rich proteins as a potential target of polyQ proteins by using whole protein sequence analysis. Furthermore, our genetic study in a fruit fly model verified that these Q-rich target proteins act as glue for facilitating polyQ protein aggregation. As far as we know, this is the first research suggesting the “glue theory” in explaining polyQ protein toxicity involving protein aggregation inside the afflicted neurons. We hope that this glue theory can be applied to other types of neurodegenerative diseases involving protein toxicity associated with protein aggregation.

Moreover, our findings provide crucial clues for developing new therapeutic strategies: either by reducing certain Q-rich target proteins or by reducing the interaction property of the interaction between polyQ and Q-rich target proteins, we may alleviate the disease symptoms or slow the progress of the disease. Notably, some of Q-rich proteins didn’t show strong interaction with polyQ proteins. So, future studies on what makes them different from other Q-rich proteins able to interact with polyQ proteins will provide deeper insight on the pathogenic mechanism of polyQ proteins.

Figures and tables

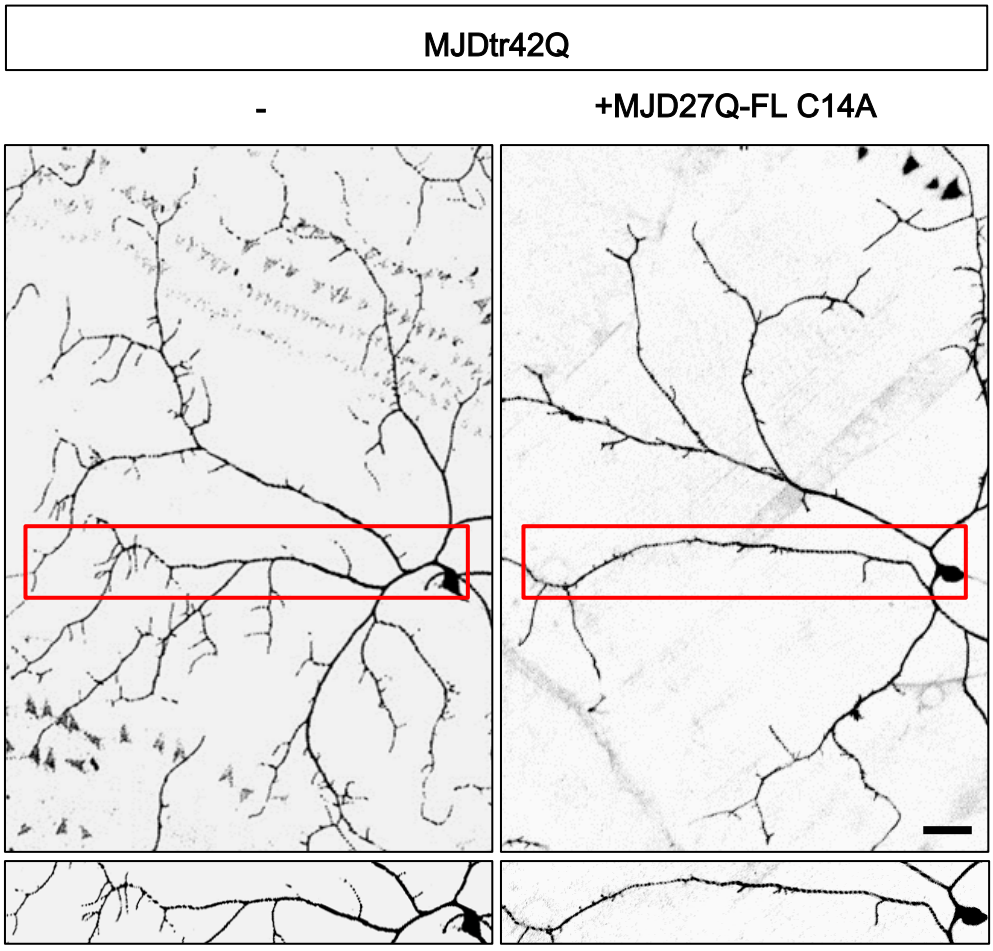

Figure 1.1 MJD27Q-FL C14A induced more dendrite defects than MJDtr42Q in class IV da neurons. *ppk*-gal4–driven expression of mCD8-GFP enabled imaging of dendrites of class IV da neurons. Each attached bottom panel is an enlarged portion of the upper panel, marked with a frame.

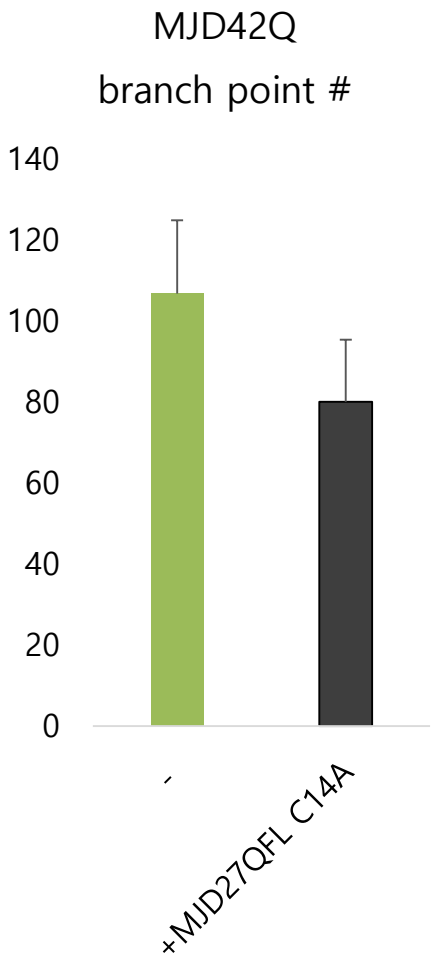

Figure 1.2 MJD27QFL C14A expression reduced the number of total dendritic branch points. The reduction of branch points of MJD27QFL C14A-expressing neurons relative to MJDtr42Q-expressing control neurons.

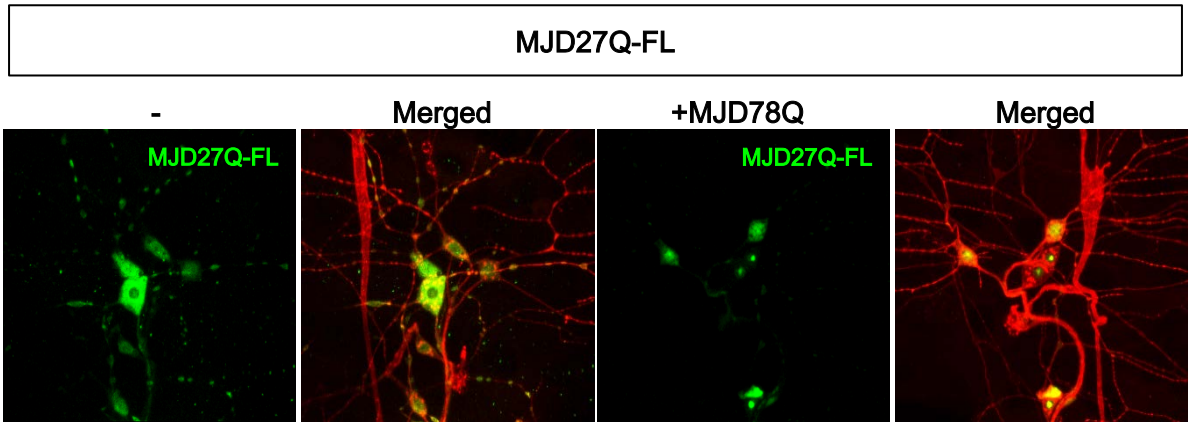

Figure 1.3 Images of polyQ proteins (MJD 27Q-FL and MJD27Q-FL + MJD78Q) in da neurons. Expanded polyQ protein (MJD78Q) trapped normal polyQ proteins (MJD27Q-FL) in aggregate forms.

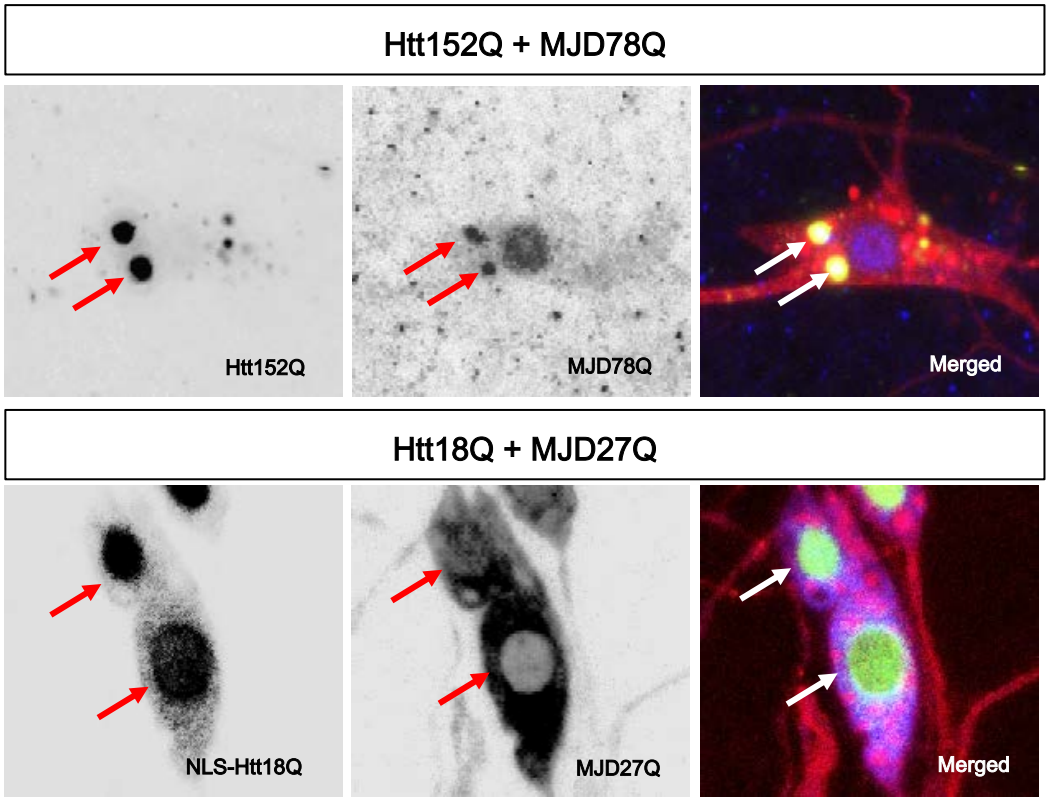

Figure 1.4 Pathogenic polyQ proteins (Htt152Q and MJD78Q) co-localize in cytoplasm in da neuron (Upper panel). Normal form of polyQ proteins (NLS-Htt18Q and MJD78Q) co-localize in nucleus in da neuron (Lower panel). Arrowheads indicate co-localizations. NLS: Nuclear Localization signal.

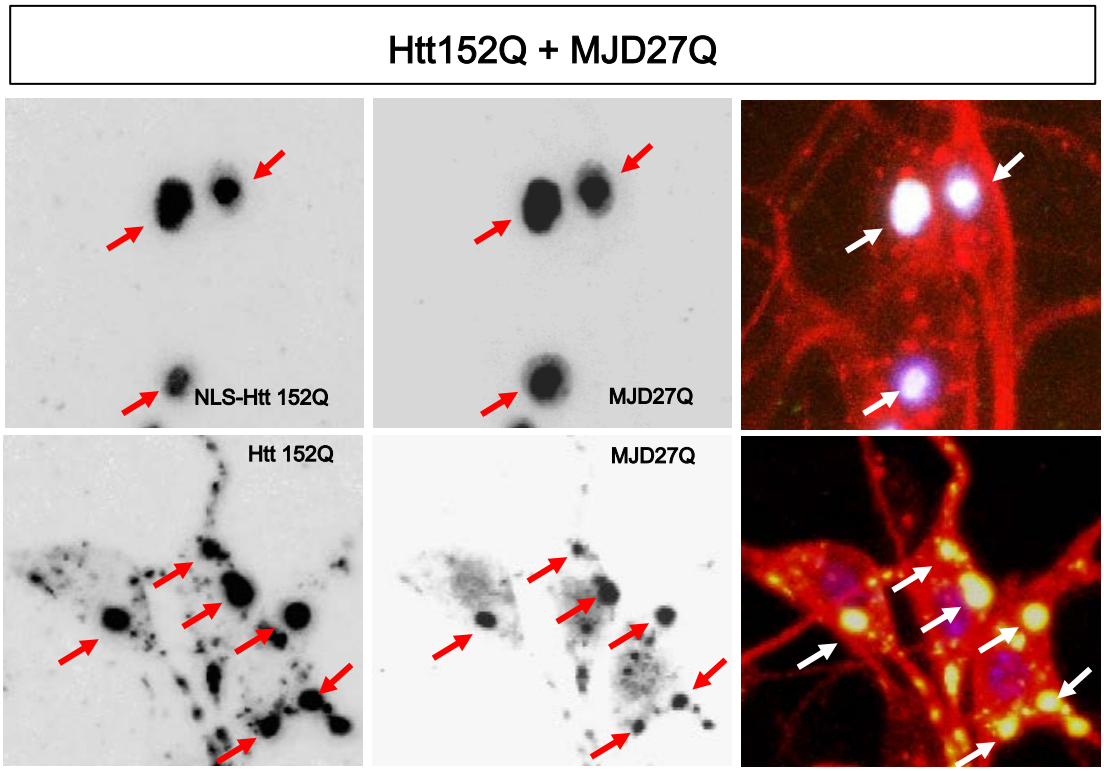

Figure 1.5 NLS-Htt152Q and MJD27Q co-localization in nucleus in da neuron (Upper panel). Htt152Q and MJD27Q co-localize in cytoplasm in da neuron (Lower panel). Target protein (MJD27Q) is trapped in pathogenic polyQ protein (NLS-Htt152Q and Htt152Q) both cytoplasm and nuclear. Arrowheads indicate co-localizations. NLS: Nuclear Localization signal.

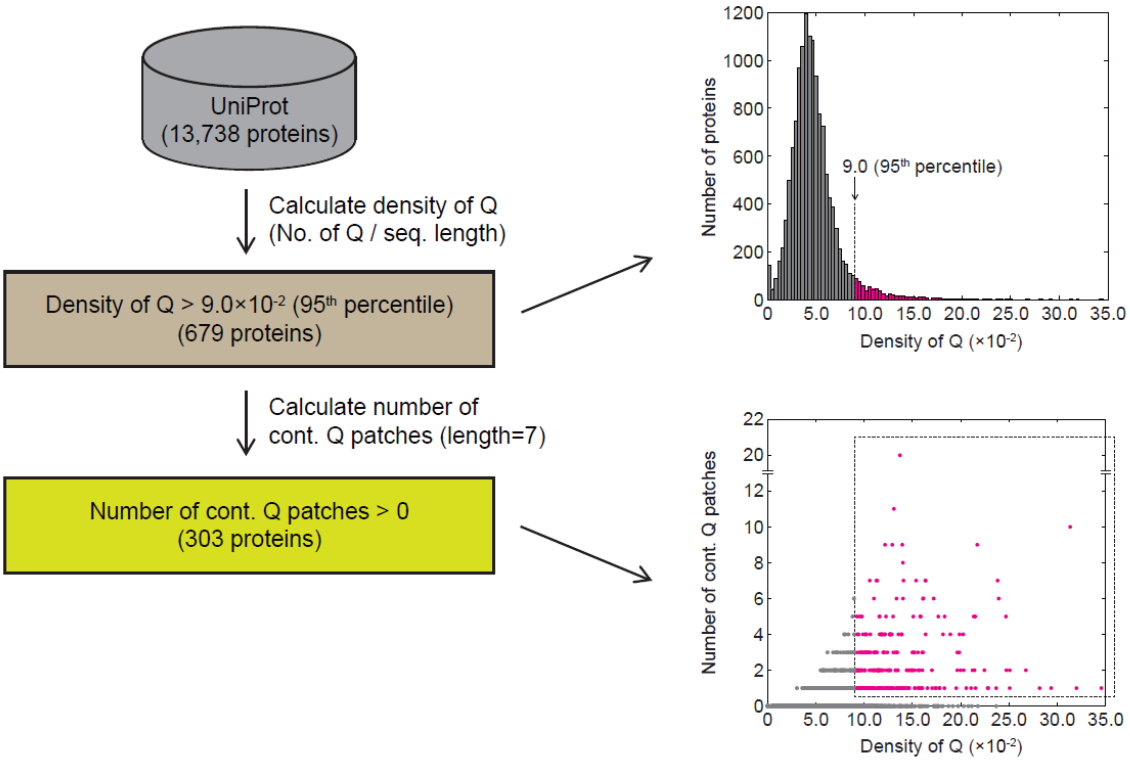

Figure 2. Canonical amino acid sequences of 13,738 proteins deposited in UniProt reference proteome for *Drosophila melanogaster* were collected (Left panel). Calculated the density of glutamine (Q) residues defined as the number of Q residues divided by sequence length (Upper Right). Calculated the number of patches composed of seven or more continuous Q residues (Lower Right). The density of Q residues > 9.0×10^{-2} (95^{th} percentile of the distribution of the density of Q residues for whole proteins)

ACC ID	Gene Symbol	description	Q count	Seq length	Q density	Continuous Q (5)	Continuous Q (6)	Continuous Q (7)
A1ZB69	Tango8	Transport and Golgi organization 8	20	88	0.344827586	2	1	1
Q7KVI2	Rdh	CG14976 gene product from transcript CG14976-RA	16	47	0.319148936	1	1	1
Q9VUB7	ptip	CG32133 gene product from transcript CG32133-RA	717	2294	0.312664449	30	14	10
Q6IHH7	CG34166	CG34166 gene product from transcript CG34166-RB	29	99	0.292929293	4	4	1
Q7KT86	CG31776	CG31776 gene product from transcript CG31776-RA	26	89	0.280898876	4	3	1
Q9VDI6	CG17271	CG17271 gene product from transcript CG17271-RB	76	281	0.266903915	4	3	2
Q0IGZ2	CG12912	CG12912 gene product from transcript CG12912-RB	28	112	0.25	2	2	2
Q9VBP6	CG6079	CG6079 gene product from transcript CG6079-RA	37	148	0.25	2	1	1
A1Z8H6	Cpr47Ee	Cuticular protein 47Ee	91	369	0.246612466	3	2	2
Q9VYT7	CG16740	CG16740 gene product from transcript CG16740-RB	240	975	0.246153846	11	9	6
Q9W3G1	CG10666	CG10666 gene product from transcript CG10666-RB	221	926	0.238660907	12	9	6
Q9VDR1	MED26	Mediator complex subunit 26	206	863	0.237543453	16	9	7
Q9I7N2	CG18787	CG18787 gene product from transcript CG18787-RB	94	398	0.236180905	7	2	1
Q9VJS1	CG16282	CG16282 gene product from transcript CG16282-RC	18	79	0.227848101	3	1	1
Q9VVS4	MED11	Mediator complex subunit 11	40	176	0.227272727	2	2	1
Q9W483	CG16772	CG16772 gene product from transcript CG16772-RB	66	269	0.223938224	3	3	2
P21519	mam	mastermind	345	1594	0.216436637	21	13	9
Q9VSN3	Cpr66D	Cuticular protein 66D	58	270	0.214814815	2	2	1
P41046	corto	CG2830 gene product from transcript CG2830-RC	118	550	0.214545455	8	6	5
Q0E8U8	CG18131	CG18131 gene product from transcript CG18131-RG	94	440	0.213636364	3	3	2
Q9W3V9	NF-YC	Nuclear factor Y-box C	128	601	0.212978369	7	5	5
Q9VA29	CG12071	CG12071 gene product from transcript CG12071-RE	123	581	0.211703959	5	4	2
Q24570	grim	CG4346 gene product from transcript CG4346-RA	29	138	0.210144928	2	1	1
Q9VWU6	CG32648	CG32648 gene product from transcript CG32648-RB	79	386	0.205194805	3	1	1
Q8I7C3	Lasp	CG3849 gene product from transcript CG3849-RB	133	657	0.202436312	5	2	2
Q9VTK5	CG7366	CG7366 gene product from transcript CG7366-RB	107	530	0.201886792	7	5	4
X2JD14	CG16366	CG16366 gene product from transcript CG16366-RA	166	828	0.199275362	7	2	2
A8JPX0	CG34364	CG34364 gene product from transcript CG34364-RE	109	550	0.198181818	5	5	4
Q08606	Trl	Trithorax-like	116	581	0.197934596	3	3	3
Q9VZA4	CG42540	CG42540 gene product from transcript CG42540-RB	99	506	0.195652604	5	4	3
Q24537	Dsp1	Dorsal switch protein 1	77	393	0.195928753	4	2	2
Q9V5Y3	CG3962	CG3962 gene product from transcript CG3962-RA	68	349	0.194842407	3	1	1
P09087	Abd-B	Abdominal B	93	493	0.188640974	5	5	4
Q9W523	ph-d	polyhomeotic distal	281	1537	0.182823582	12	10	5
P02833	Antp	Antennapedia	69	378	0.182539683	3	2	1
P39769	ph-p	polyhomeotic proximal	288	1689	0.181246067	11	8	4
Q8T3Y1	CG17440	CG17440 gene product from transcript CG17440-RA	66	366	0.177595628	1	1	1
Q9W4V4	CG14418	CG14418 gene product from transcript CG14418-RB	58	327	0.177370031	3	2	1
Q9VQK1	CG17266	CG17266 gene product from transcript CG17266-RA	107	607	0.176276771	5	5	5
Q9VNT4	CG14469	CG14469 gene product from transcript CG14469-RC	28	161	0.173913043	2	1	1
M9PET2	tow	target of wingless	78	461	0.172949002	5	5	1
A0A0B4KGW2	sr	stripe	218	1271	0.171518489	11	8	5
Q9W0P3	MED30	Mediator complex subunit 30	64	376	0.169811321	4	3	1
Q8INY6	CG6674	CG6674 gene product from transcript CG6674-RB	83	489	0.169734151	5	3	2
A0A0B4LF62	CG44314	CG44314 gene product from transcript CG44314-RB	16	97	0.164948454	1	1	1
A0A0B4K051	CG11873	CG11873 gene product from transcript CG11873-RB	490	3003	0.163170163	19	12	7
Q9VWA0	CG17233	CG17233 gene product from transcript CG17233-RG	239	1466	0.163199932	15	12	4
A8DYV5	Ncoa6	CG14023 gene product from transcript CG14023-RD	402	2467	0.162960953	24	15	7
A0A0B4KFE1	CG10643	CG10643 gene product from transcript CG10643-RF	263	1636	0.160866269	13	8	5
Q8SWR6	Atx2	Ataxin-2	174	1084	0.160516606	4	3	3
Q9VRY4	velo	veloren	294	1833	0.160392799	12	9	5
Q9VUQ6	AGO2	Argonaute 2	194	1214	0.159802306	2	1	1
M9PFU2	Crtc	CREB-regulated transcription coactivator	142	889	0.159730034	10	8	2
Q9VFT4	rin	rasputin	110	690	0.15942029	5	3	3
Q9VDZ3	sqz	squeeze	86	535	0.160747606	4	1	1
A0A0B4KHZ2	sbs	six-banded	264	1606	0.164359912	11	7	5
Q9VU11	CG10969	CG10969 gene product from transcript CG10969-RA	110	697	0.157819226	2	2	1

Table 1. List of possible Q-rich target proteins in Drosophila melanogaster.

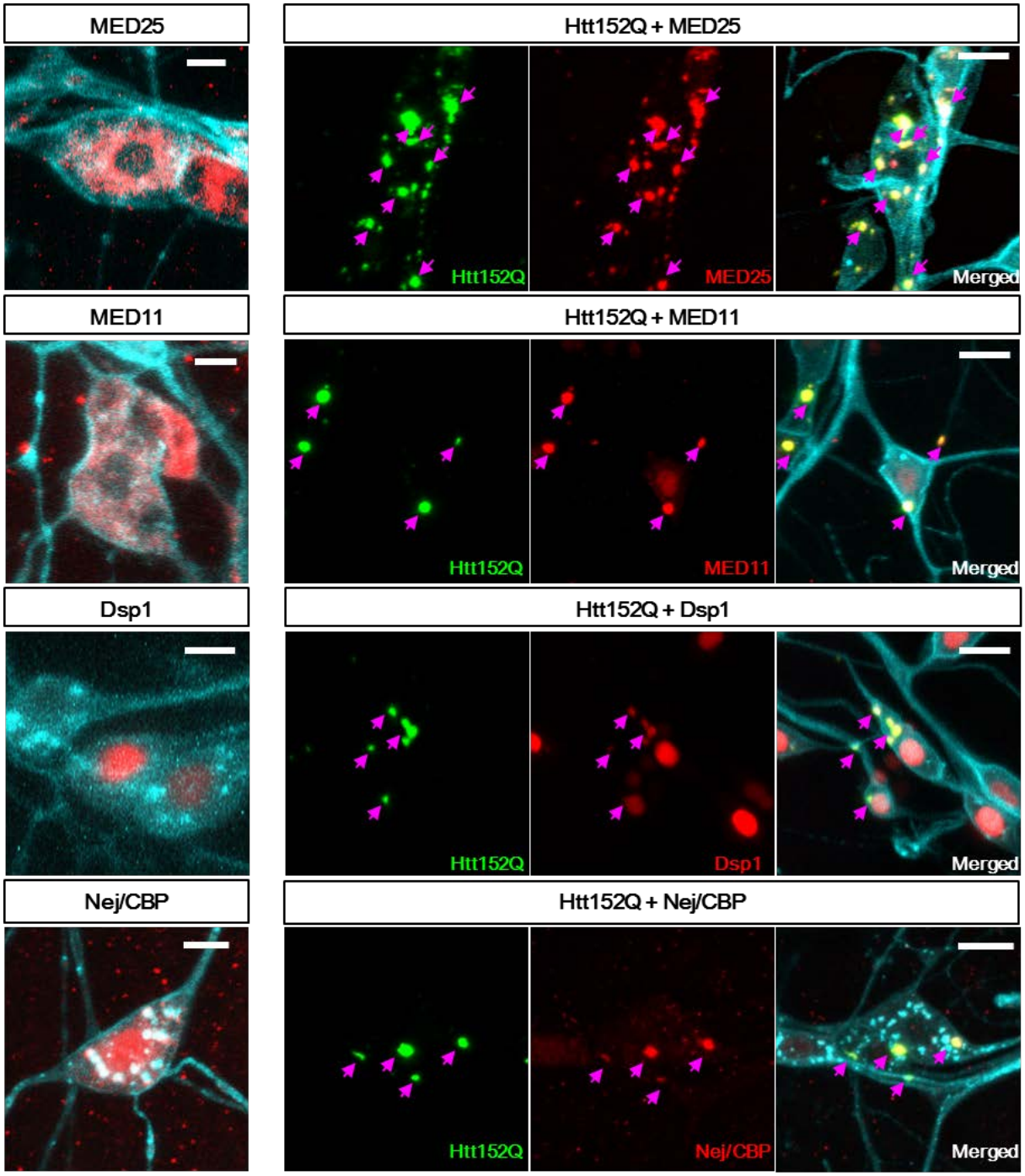

Figure 3. Images of co-localization between possible Q-rich target proteins (MED25, MED11, Dsp1, nej/CBP) and pathogenic polyQ protein (Htt152Q). (Left) Localization of Q-rich target proteins. (Right) Co-express between pathogenic polyQ protein (Htt152Q) and target proteins (MED11, MED25, Dsp1 and CBP). Arrowheads indicate co-localization.

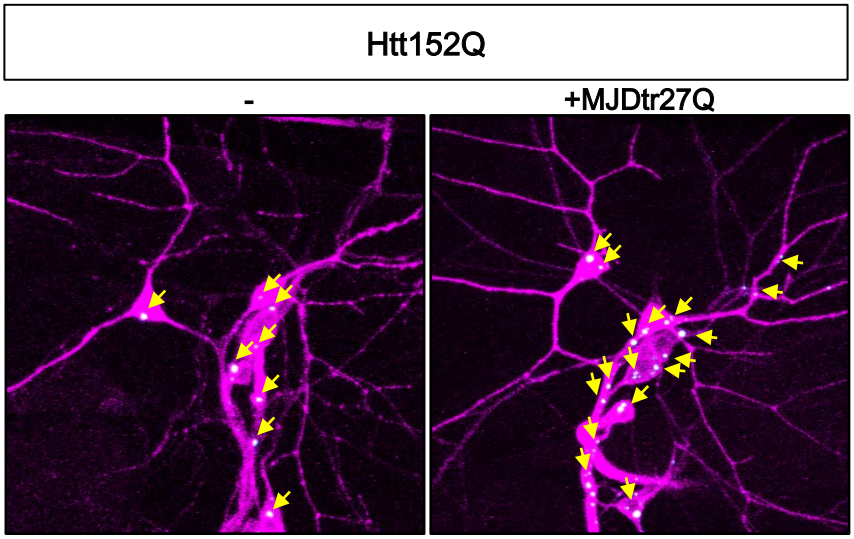

Figure 4.1 Overexpression of target protein (MJDtr27Q) with pathogenic polyQ protein (Htt152Q) increase aggregate numbers. Arrowhead indicated aggregates.

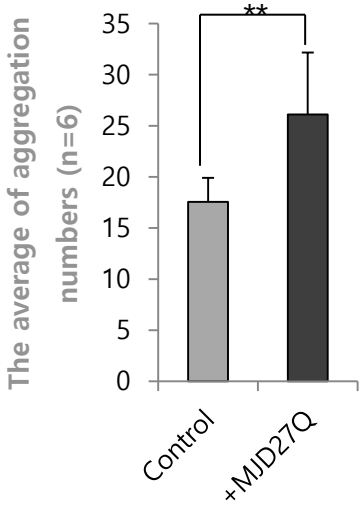

Figure 4.2 Quantification of aggregate numbers in class IV da neurons expressing denoted transgenes (control (Htt152Q), Htt152Q+MJD27Q). Bars indicate mean ± SD; *n* = 6; ***P* < 0.01 (Student's unpaired *t* test) relative to control.

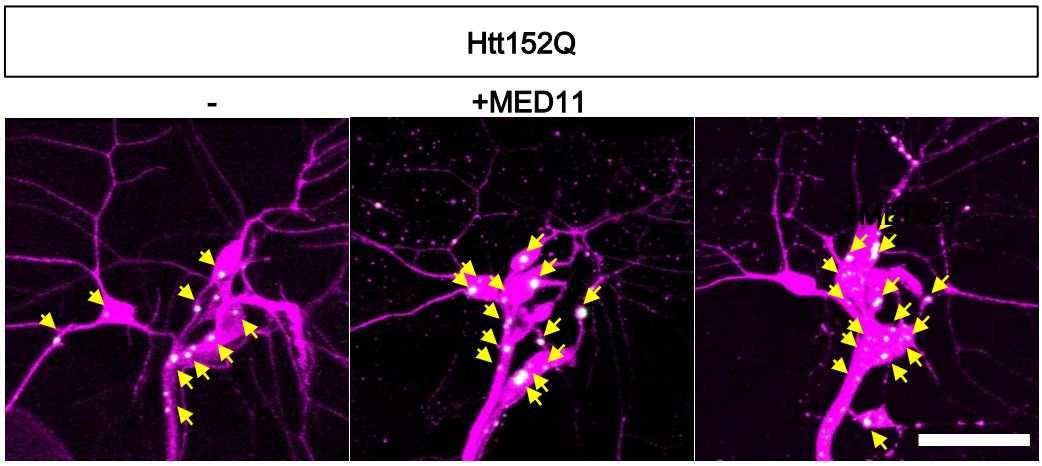

Figure 4.3 Overexpression of target protein (MED11 and MED25) with pathogenic polyQ protein (Htt152Q) increase aggregate numbers. Arrowhead indicated aggregates.

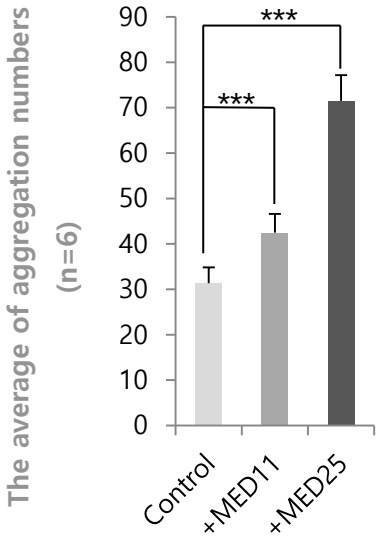

Figure 4.4 Quantification of aggregate numbers in class IV da neurons expressing denoted transgenes (control (Htt152Q), Htt152Q+MED11 and Htt152Q+MED25). Bars indicate mean ± SD; $n = 6$; ***$P < 0.001$ (Student's unpaired t test) relative to control.

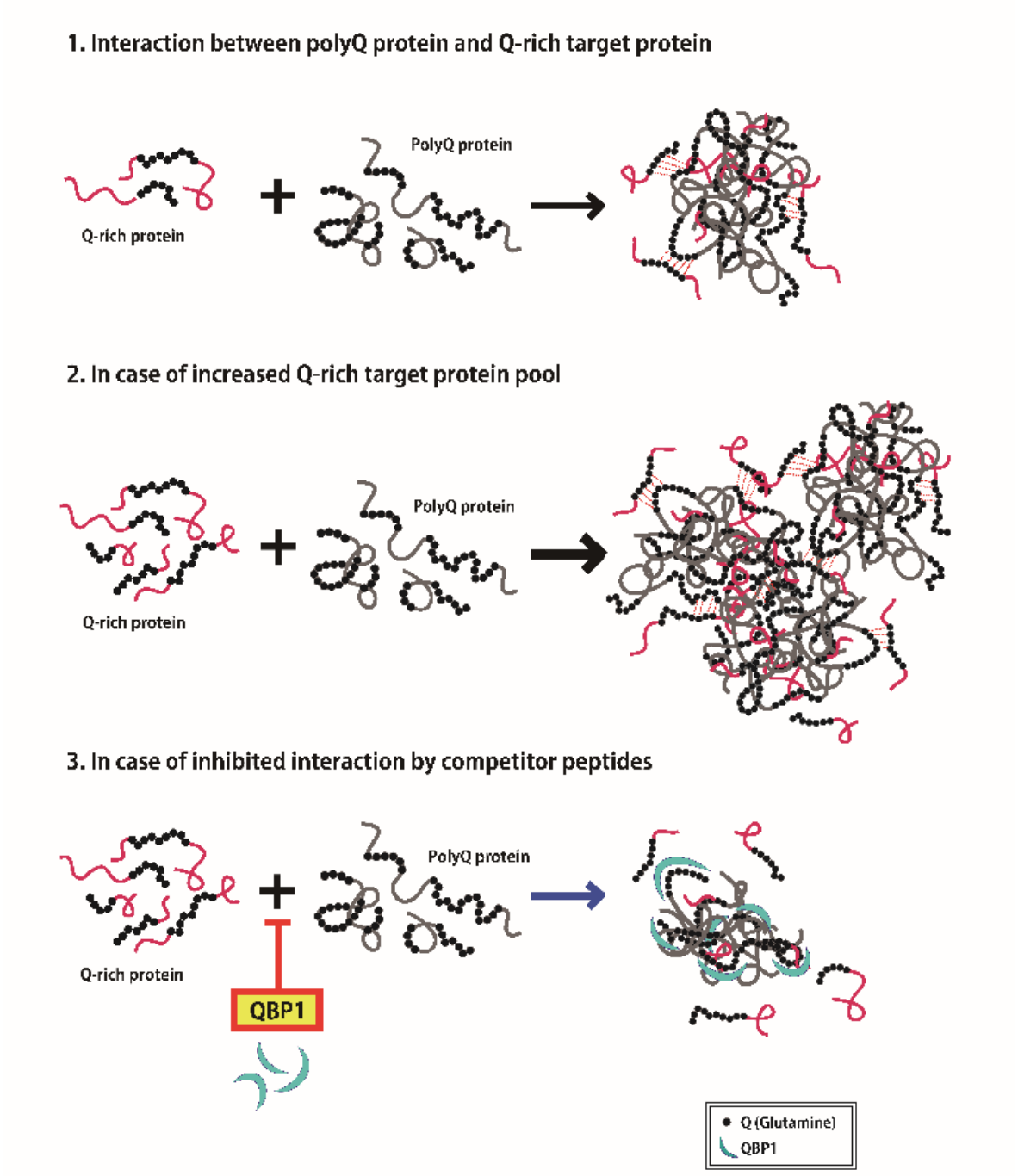

Figure 5.1 The proposed schematic diagram for the key implication of our study; (1) Q-rich target proteins interact with pathogenic polyQ proteins (2) by working as glue (increasing interaction property), (3) and possible strategy of preventing interaction opportunity using structural inhibitor, QBP1.

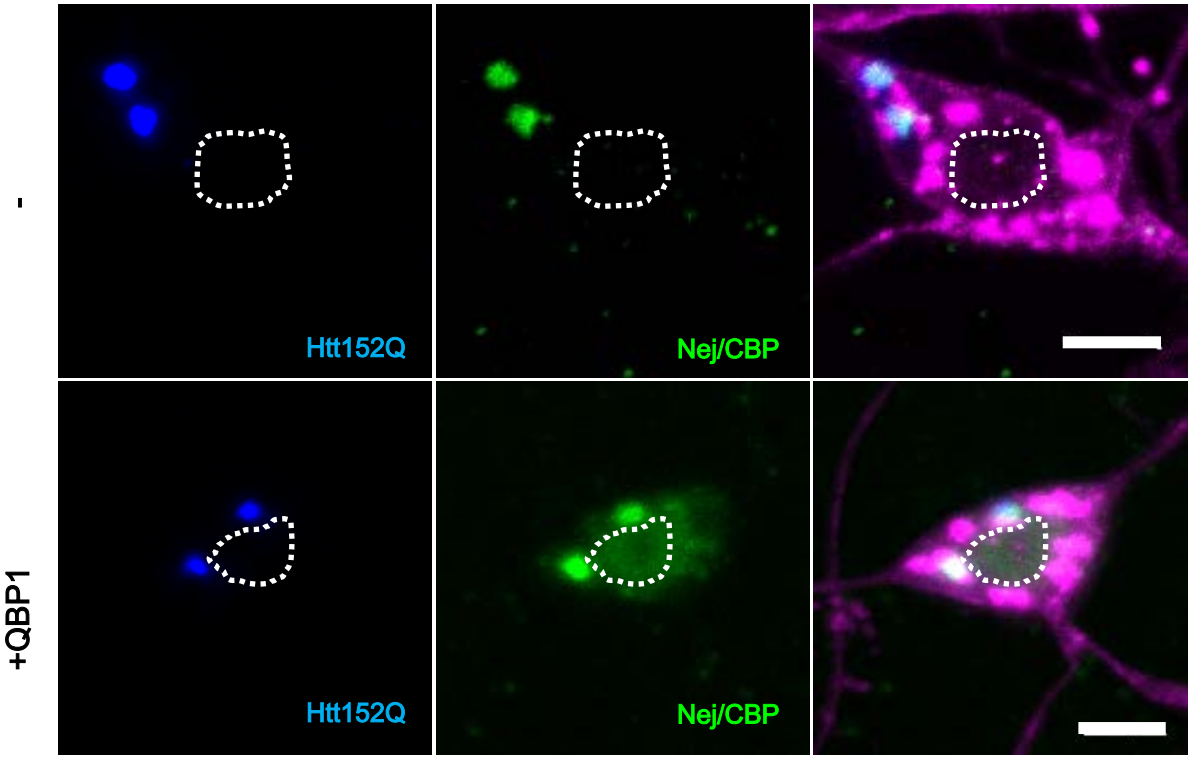

Figure 5.2 Localization of CBP in *Drosophlia* da neurons. Pathogenic polyQ (Htt152Q) interacts with CBP in cytoplasm (Upper panel). QBP1 inhibit aggregate formation in da neurons of Htt152Q+CBP (Lower panel). CBP seems to be released from pathogenic polyQ protein (Htt152Q).

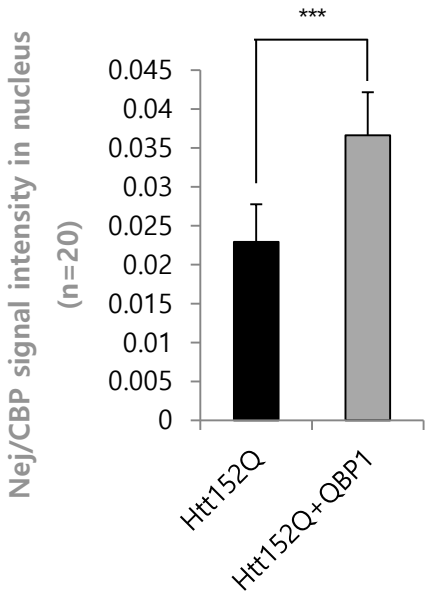

Figure 5.3 Quantification of CBP signal intensity in nucleus expressing denoted transgenes (control (Htt152Q+CBP), Htt152Q+CBP+QBP1). Bars indicate mean ± SD; *n* = 20; ****P* < 0.001 (Student's unpaired *t* test) relative to control.

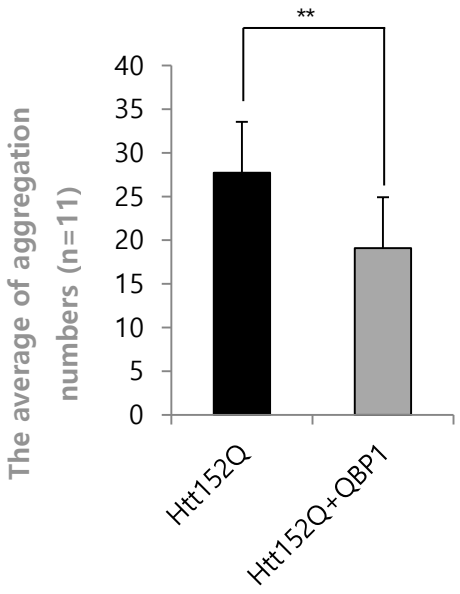

Figure 5.4 Quantification of aggregate numbers in da neurons expressing denoted transgenes (control (Htt152Q+CBP), Htt152Q+CBP+QBP1). Bars indicate mean ± SD; *n* = 20; ***P* < 0.01 (Student's unpaired *t* test) relative to control.

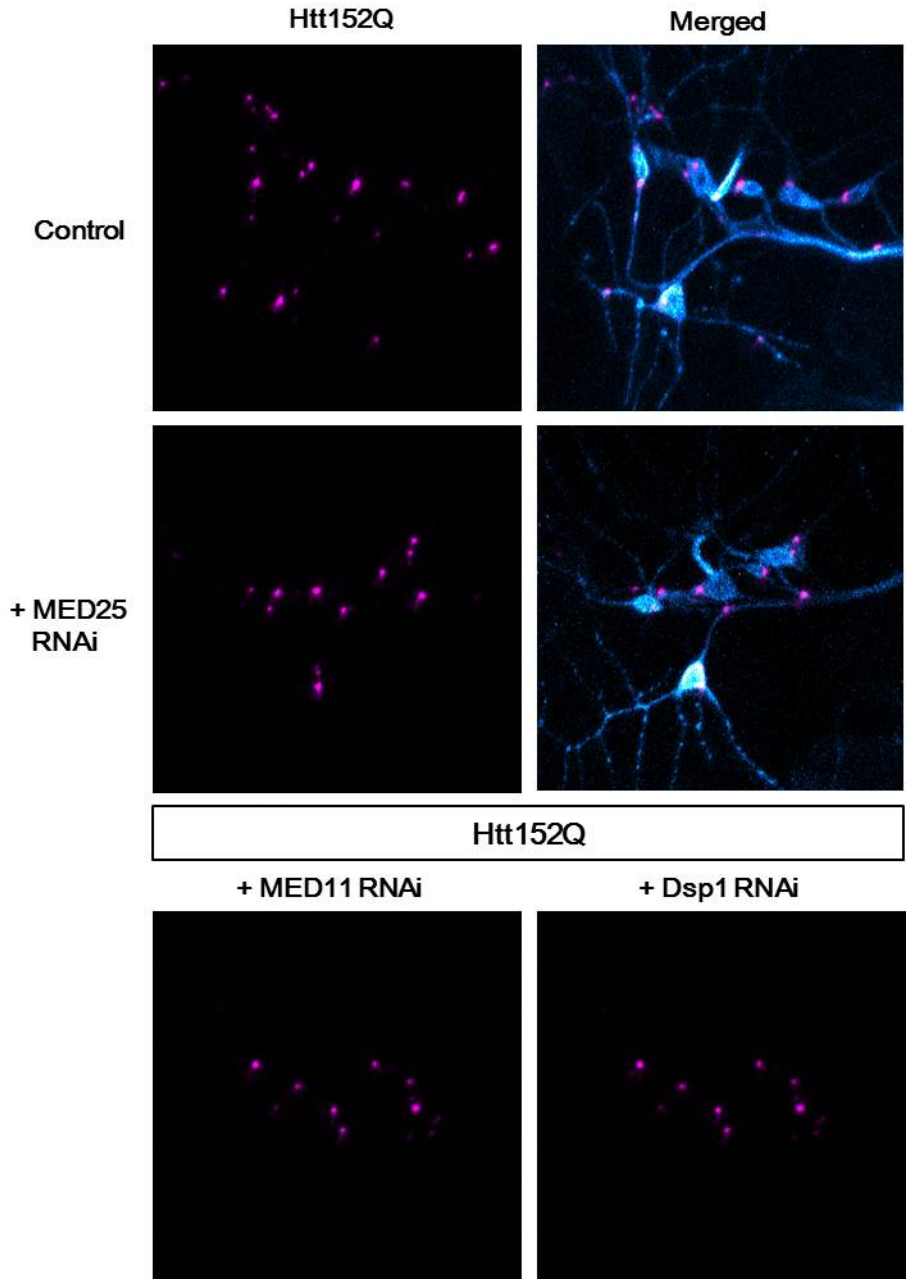

Figure 6.1 RNA interference of target protein (MED25 RNAi, MED11 RNAi and Dsp1 RNAi) with pathogenic polyQ protein (Htt152Q) decrease aggregate numbers.

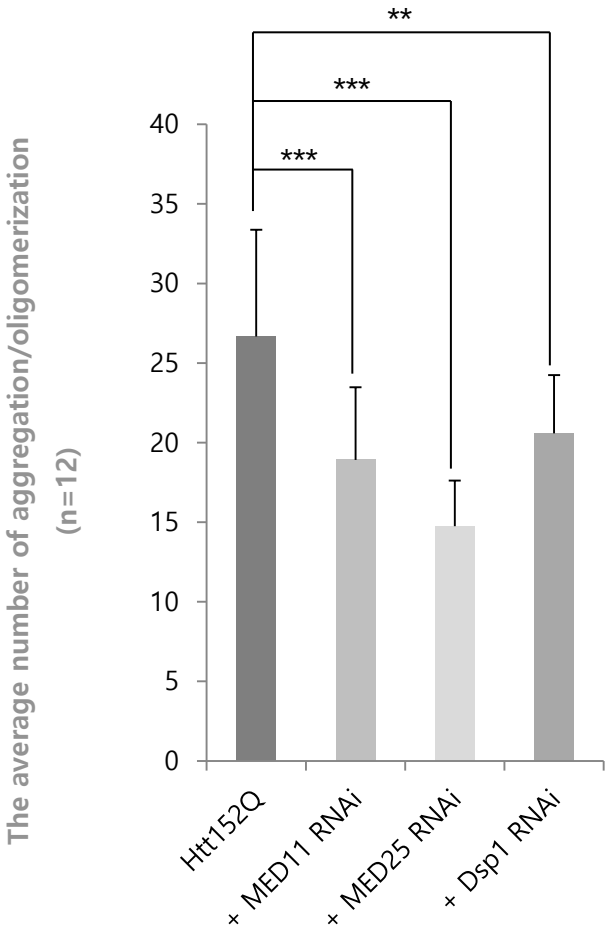

Figure 6.2 Quantification of aggregate numbers in da neurons expressing denoted transgenes (Htt152Q, Htt152Q+MED11 RNAi, Htt152Q+MED25 RNAi, Htt152Q+Dsp1 RNAi). Bars indicate mean ± SD; $n = 12$; ***$P < 0.001$ (Student's unpaired t test) relative to control.

ACC ID	Gene Symbol	description	Q count	Seq length	Q density	Continuous Q (5)	Continuous Q (6)	Continuous Q (7)	nucleus
P0CG23	ZNF883	zinc finger protein 883	174	659	0.264036419	3	1	1	0
Q96RN5	MED15	mediator complex subunit 15	157	788	0.199238579	7	5	4	1
O15409	FOXP2	forkhead box P2	127	715	0.177622378	2	2	2	1
P20226	TBP	TATA box binding protein	60	339	0.17699115	1	1	1	0
O15405	TOX3	TOX high mobility group box family member 3	99	576	0.171875	2	1	1	1
Q8IZL2	MAML2	mastermind-like 2 (Drosophila)	194	1156	0.167820069	3	3	3	1
Q96JK9	MAML3	mastermind-like 3 (Drosophila)	173	1138	0.15202109	3	3	3	1
Q6ZW49	PAXIP1	PAX interacting (with transcription-activation domain) protein 1	150	1069	0.140318054	7	6	5	1
O94916	NFAT5	nuclear factor of activated T-cells 5, tonicity-responsive	214	1531	0.139777923	3	2	2	1
Q8WYJ4	PHLDA1	pleckstrin homology-like domain, family A, member 1	56	401	0.139650873	1	1	1	0
P78424	POU6F2	POU class 6 homeobox 2	95	691	0.13748191	1	1	1	1
P78364	PHC1	polyhomeotic homolog 1 (Drosophila)	135	1004	0.134462151	2	1	1	1
Q9H334	FOXP1	forkhead box P1	91	677	0.134416544	2	2	1	1
Q96EK4	THAP11	THAP domain containing 11	41	314	0.130573248	1	1	1	0
P50553	ASCL1	achaete-scute family bHLH transcription factor 1	30	236	0.127118644	1	1	1	1
Q14686	NCOA6	nuclear receptor coactivator 6	245	2063	0.118759089	2	2	2	1
Q15714	TSC22D1	TSC22 domain family, member 1	126	1073	0.117427773	1	1	1	1
Q2M2I8	AAK1	AP2 associated kinase 1	112	961	0.116545265	2	2	2	0
Q6Y7W6	GIGYF2	GRB10 interacting GYF protein 2	151	1299	0.116243264	5	4	3	0
P20265	POU3F2	POU class 3 homeobox 2	50	443	0.112866817	1	1	1	1
Q92793	CREBBP	CREB binding protein	268	2442	0.10974611	2	1	1	1
Q9Y2K5	R3HDM2	R3H domain containing 2	107	976	0.109631148	1	1	1	1
Q96L91	EP400	E1A binding protein p400	341	3159	0.107945552	1	1	1	0
O60885	BRD4	bromodomain containing 4	147	1362	0.107929515	3	1	1	1
Q5SZQ8	CELF3	CUGBP, Elav-like family member 3	50	465	0.107526882	1	1	1	1
Q9Y5J6	TIMM10B	translocase of inner mitochondrial membrane 10 homolog B (yeast)	11	103	0.106796117	1	1	1	0
P54252	ATXN3	ataxin 3	38	364	0.104395604	1	1	1	1
Q8TF68	ZNF384	zinc finger protein 384	60	577	0.103986135	1	1	1	1
Q9Y6Q9	NCOA3	nuclear receptor coactivator 3	146	1424	0.10252809	2	1	1	1
Q9NSY1	BMP2K	BMP2 inducible kinase	116	1161	0.099913867	1	1	1	0
Q13495	MAMLD1	mastermind-like domain containing 1	77	774	0.099483204	2	2	2	1
O14910	LIN7A	lin-7 homolog A (C. elegans)	23	233	0.098712446	1	1	1	0
Q01826	SATB1	SATB homeobox 1	75	763	0.098296199	1	1	1	1
Q8WXI8	CHERP	calcium homeostasis endoplasmic reticulum protein	90	916	0.098253275	1	1	1	0
Q9Y2K2	SIK3	SIK family kinase 3	123	1263	0.097387173	1	1	1	0
Q93074	MED12	mediator complex subunit 12	212	2177	0.097381718	5	4	3	1
O14497	ARID1A	AT rich interactive domain 1A (SWI-like)	219	2285	0.095842451	2	1	1	1
Q8IZD4	DCP1B	decapping mRNA 1B	59	617	0.095623987	1	1	1	1
P0CG43	#N/A	#N/A	37	387	0.095607235	1	1	1	0
Q10571	MN1	meningioma (disrupted in balanced translocation) 1	124	1320	0.093939394	3	2	1	0
Q4VCS5	AMOT	angiomotin	100	1084	0.092250923	2	2	2	0
C9JC47	FAM157A	family with sequence similarity 157, member A	35	383	0.091383812	1	1	1	0
Q68DE3	KIAA2018	KIAA2018	203	2245	0.090423163	1	1	1	1
Q8NFD5	ARID1B	AT rich interactive domain 1B (SWI1-like)	201	2236	0.089892665	1	1	1	0
P54253	ATXN1	ataxin 1	73	815	0.089570552	2	2	2	1
Q9P0K8	FOXJ2	forkhead box J2	51	574	0.088850174	1	1	1	1
P0CG42	FAM157B	family with sequence similarity 157, member B	34	384	0.088541667	1	1	1	0
Q9UGI6	KCNN3	potassium channel, calcium activated intermediate/small conductance subfamily N alpha, member 3	64	736	0.086956522	3	2	2	0
Q6PJG2	ELMSAN1	ELM2 and Myb/SANT-like domain containing 1	89	1045	0.085167464	2	2	1	0
Q9NQV6	PRDM10	PR domain containing 10	97	1147	0.084568439	1	1	1	1
Q13950	RUNX2	runt-related transcription factor 2	44	521	0.084452975	1	1	1	0
Q5T953	IER5L	Immediate early response 5-like	34	404	0.084158416	1	1	1	0
O95104	SCAF4	SR-related CTD-associated factor 4	96	1147	0.0836966	1	1	1	0
O14686	KMT2D	lysine (K)-specific methyltransferase 2D	454	5537	0.081993659	19	14	10	1
P19484	TFEB	transcription factor EB	39	476	0.081932773	1	1	1	1
B1AL88	FAM155A	family with sequence similarity 155, member A	37	458	0.080786026	2	2	1	0
Q99626	CDX2	caudal type homeobox 2	25	313	0.079872204	1	1	1	0

Table 2. List of possible Q-rich target proteins in Human.

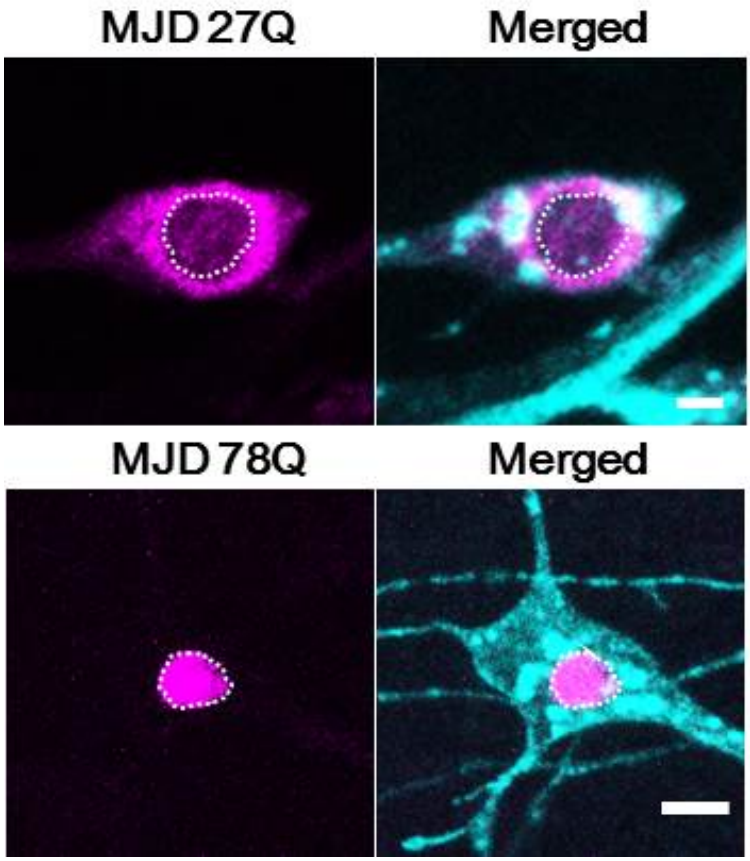

Supplementary figure 1.1 Localization of Ataxin-3 (MJD/SCA3) expressions in da neurons. MJD27 localizes to the cytoplasm (Upper panel) MJD78Q localizes to the nucleus (Lower panel). Dotted lines appear nucleus.

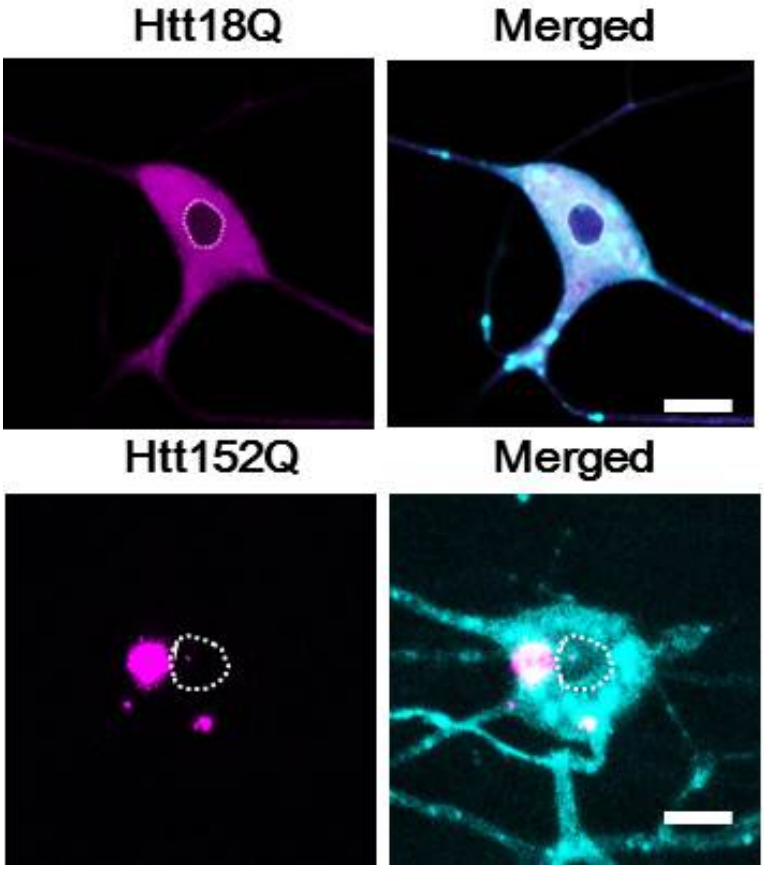

Supplementary figure 1.2 Localization of Huntingtin (Htt) expressions in da neurons. Htt18Q (Upper panel) and Htt152Q (Lower panel) localize to the cytoplasm. Dotted lines appear nucleus.

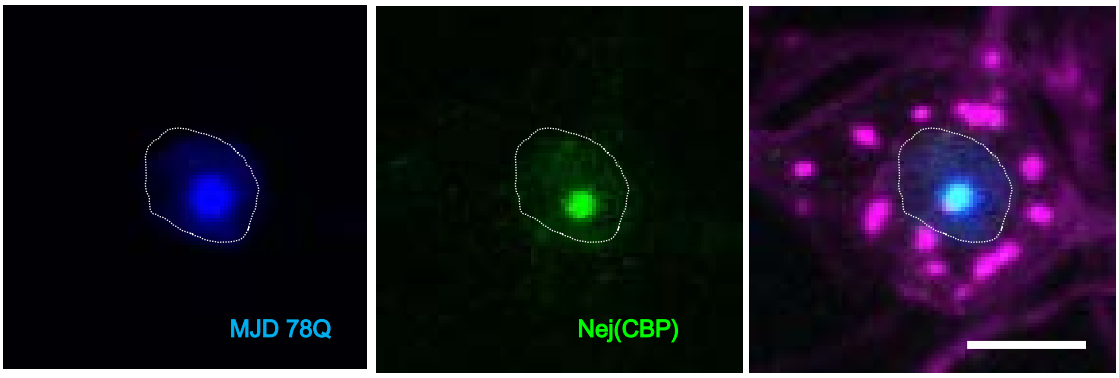

Supplementary figure 2. Confocal images of nej/CBP expressions with MJD78Q in da neurons. Dotted lines appear nucleus.

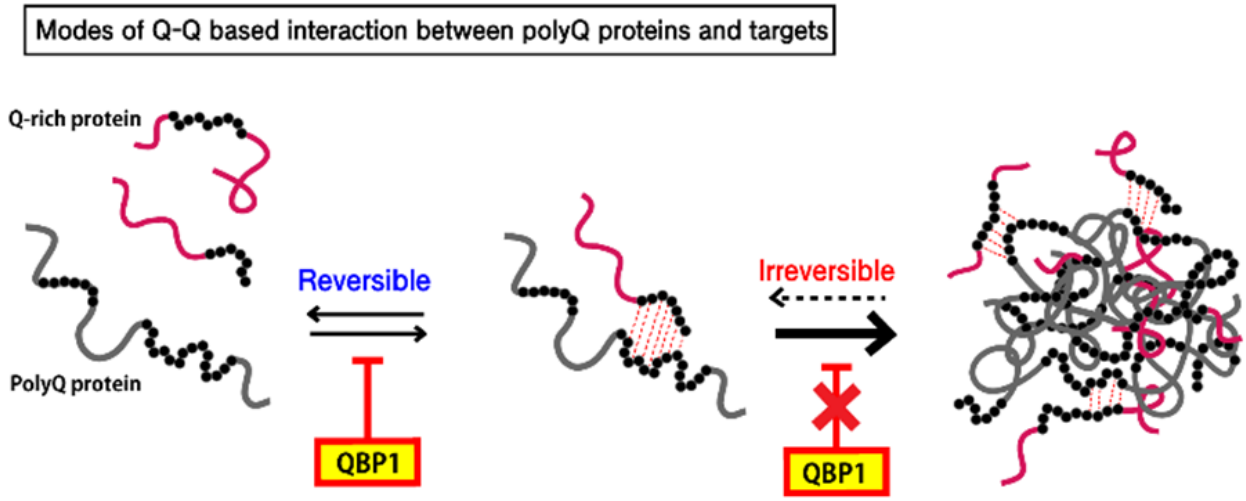

Supplementary figure 3.1 The schematic diagram for sequestering or trapping the plausible targets of the polyQ aggregates, and their transition modes from reversible mode to irreversible mode.

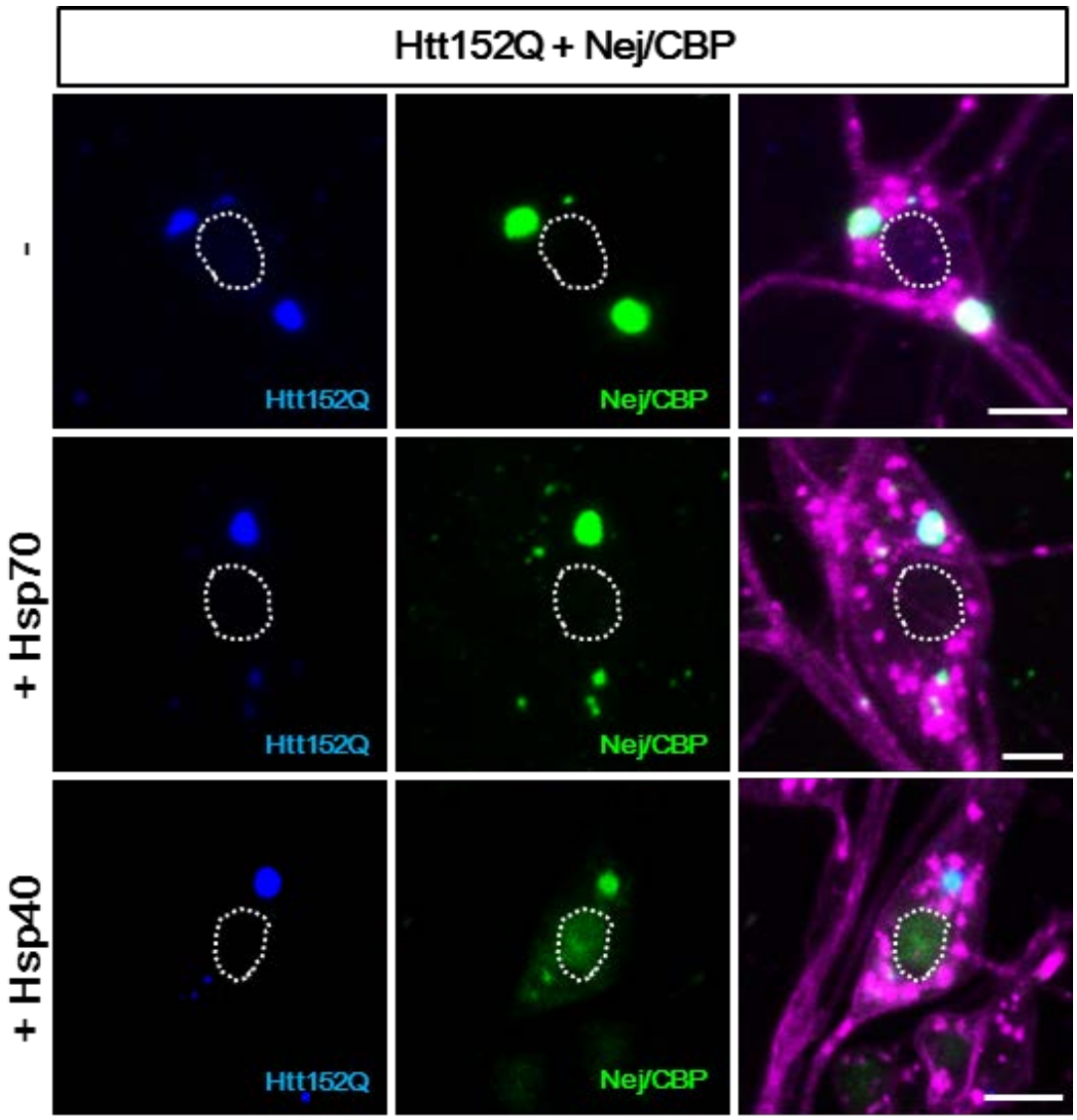

Supplementary figure 3.2 Heat shock proteins prevent aggregate formation between pathogenic polyQ and target protein. Co-localiztion of pathogenic polyQ protein (Htt152Q) and Q-rich target protein (nej/CBP) (Upper panel). Co-expressed Hsp70 with Htt152Q + nej/CBP (Middle panel), and Hsp40 with Htt152Q+nej/CBP (Lower panel) in neurons.

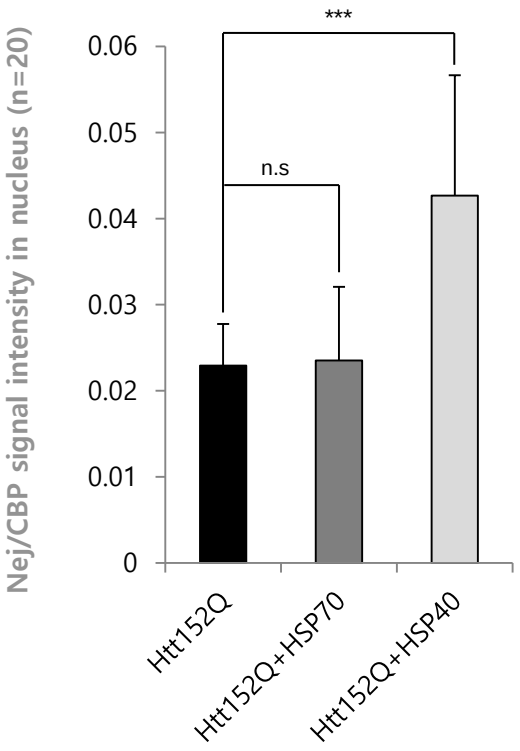

Supplementary figure 3.3 Quantification of nej/CBP signal intensity in nucleus expressing denoted transgenes (control (Htt152Q+nej/CBP), Htt152Q+nej/CBP+HSP70, Htt152Q+nej/CBP+HSP40). Bars indicate mean ± SD; $n = 20$; ***$P < 0.001$ (Student's unpaired *t* test) relative to control.

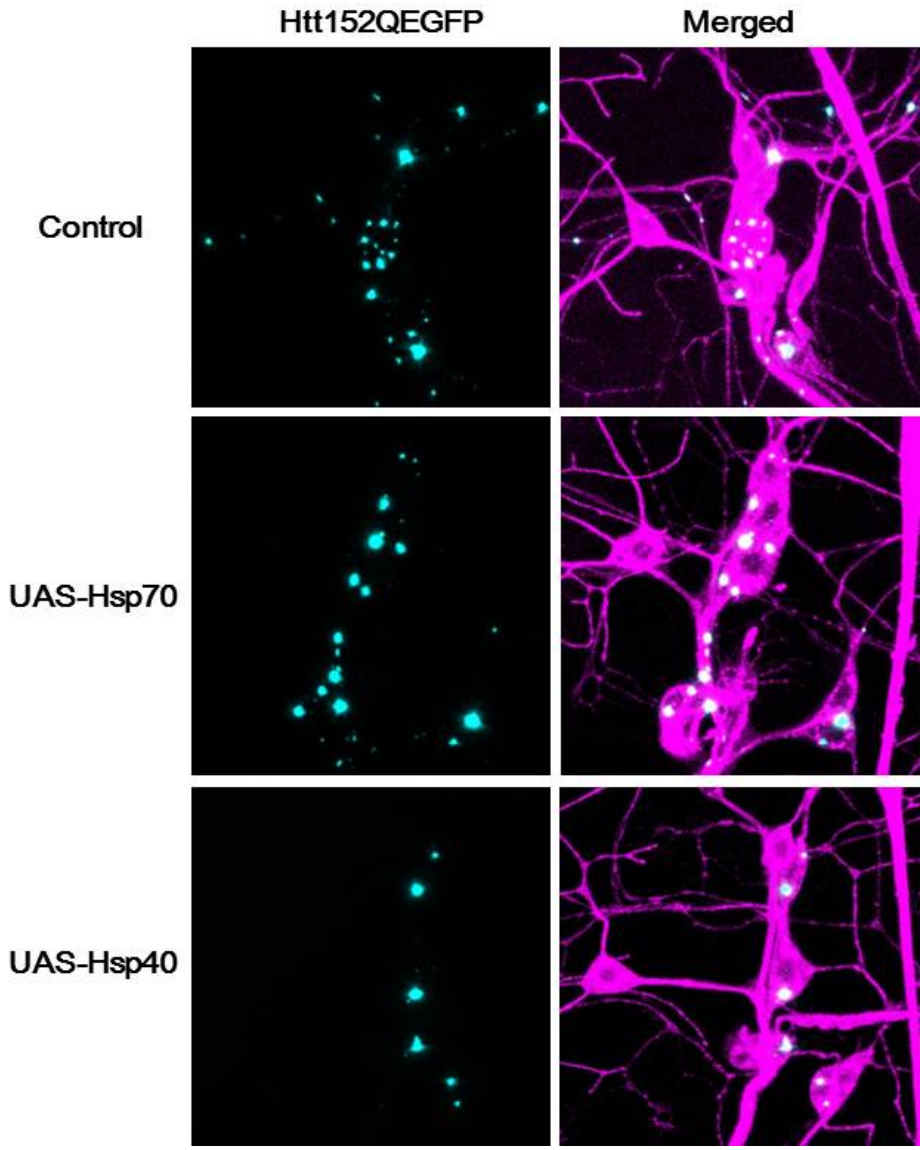

Supplementary figure 4.1 Effects of chaperones on pathogenic polyQ protein (Htt152Q). Confocal images of aggregate formation in neurons. Htt152Q (Upper panel), Htt152Q with Hsp70 (Middle panel), and Htt152Q with Hsp40 (Lower panel). Co-expression of Hsp40 significantly reduced huntingtin aggregation

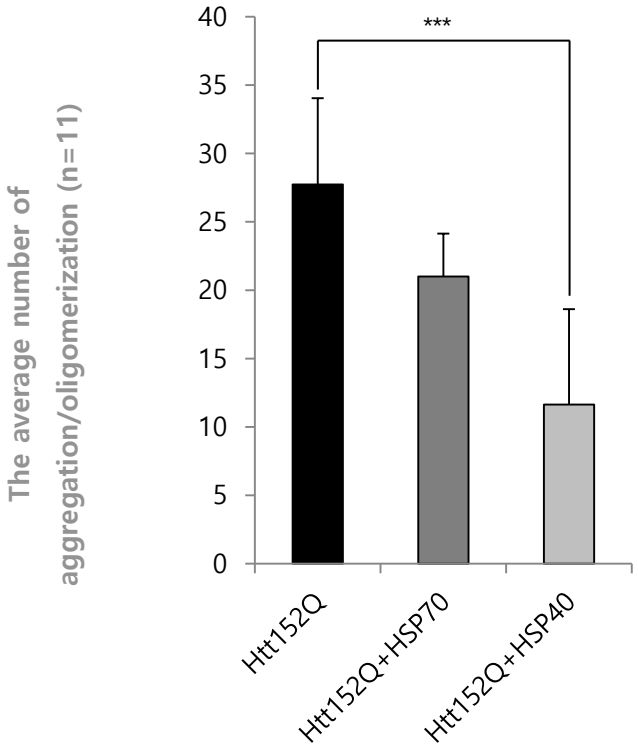

Supplementary figure 4.2 Quantification of the aggregate formation numbers in neurons expressing denoted transgenes (control (Htt152Q+nej/CBP), Htt152Q+nej/CBP+HSP70, Htt152Q+nej/CBP+HSP40). Bars indicate mean ± SD; $n = 11$; ***$P < 0.001$ (Student's unpaired *t* test) relative to control.

References

Zoghbi, H. Y. & Orr, H. T. Glutamine repeats and neurodegeneration. Annu Rev Neurosci 23, 217–247 (2000).

Orr, H. T. & Zoghbi, H. Y. Trinucleotide repeat disorders. Annu Rev Neurosci 30, 575–621 (2007).

Arrasate, M., Mitra, S., Schweitzer, E. S., Segal, M. R. & Finkbeiner, S. Inclusion body formation reduces levels of mutant huntingtin and the risk of neuronal death. Nature 431, 805–810 (2004).

Ross, C. A. & Poirier, M. A. Protein aggregation and neurodegenerative disease. Nat Med 10 Suppl, S10–17 (2004).

Lee, S. B., Bagley, J. A., Lee, H. Y., Jan, L.Y. & Jan, Y. N. Pathogenic polyglutamine proteins cause dendrite defects associated with specific actin cytoskeletal alterations in Drosophila. Proc. Natl. Acad. Sci. 108, 16795-16800 (2011).

McCampbell, A. et al. CREB-binding protein sequestration by expanded polyglutamine. Hum Mol Genet 9, 2197–2202 (2000).

Paulson, H. L. et al. Intranuclear inclusions of expanded polyglutamine protein in spinocerebellar ataxia type 3. Neuron 19, 333–344 (1997).

Warrick, J. M., Morabito, L. M., Bilen, J., Gordesky-Gold, B., Faust, L. Z., Paulson, H. L. & Bonini, N. M. Ataxin-3 suppresses polyglutamine neurodegeneration in Drosophila by a ubiquitin-associated mechanism. Mol Cell. 18, 37-48 (2005)

Olzscha, H. et al. Amyloid-like aggregates sequester numerous metastable proteins with essential cellular functions. Cell 144, 67–78 (2011).

Tait, D., Riccio, M., Sittler, A., Scherzinger, E., Santi, S. et al. Ataxin-3 is transported into the nucleus and associates with the nuclear matrix. Hum. Mol. Genet. 7, 991-997 (1998).

Nucifora, F. C., Jr., Sasaki, M., Peters, M. F., Huang, H., Cooper, J. K., Yamada, M., Takahashi, H., Tsuji, S. Troncoso, J., Dawson, W. L., Dawson, T. M., & Ross, C. A. Interference by huntingtin and Atrophin-1 with CBP-mediated Transcription Leading to Cellular Toxicity. Science 291, 2423-2428 (2001).

Steffan, J. S., Bodai, L., Pallos, J., Poelman, M., McCampbell, A., Apostol, B. L., Kazantsev, A., Schmidt, E., Zhu, Y. Z., Greenwald, M., et al. Histonedeacetylase inhibitors arrest polyglutamine-dependent neurogeneration in Drosophila. Nature 413, 739-743 (2001).

Steffan, J. S., Kazantsev, A., Spasic-Boskovic, O., Greenwald, M., Zhu, Y. Z., Gohler, H., Wanker, E. E., Bates, G. P., Housman, D.E., Thompson L,M,. The Huntington's disease protein interacts with p53 and CREB-binding protein and represses transcription. Proc Natl Acad Sci U S A. 97, 6763-8 (2000).

Popiel, H. A., Nagai, Y., Fujikake, N. & Toda, T. Protein transduction domain-mediated delivery of QBP1 suppresses polyglutamine-induced neurodegeneration in vivo. Mol Ther. 15, 303-9 (2007)

Popiel, H.A., Takeuchi, T., Burke, J. R., Strittmatter, W. J., Toda, T., Wada, K. & Nagai, Y. Inhibition of protein misfolding/aggregation using polyglutamine binding peptide QBP1 as a therapy for the polyglutamine diseases. Neurotherapeutics. 10, 440-6 (2013).

Popiel, H. A., Burke, J. R., Strittmatter, W. J, Oishi, S., Fujii, N., Takeuchi, T., Toda, T., Wada, K., Nagai, Y. The Aggregation Inhibitor Peptide QBP1 as a Therapeutic Molecule for the Polyglutamine Neurodegenerative Diseases. J Amino Acids . J Amino Acids. 2011: 265084 (2011).

Kole, R., Krainer, A. R. & Altman, S. RNA therapeutics: beyond RNA interference and antisense oligonucleotides. Nat Rev Drug Discov 11, 125-40 (2011)

Zhou, H,, Li, S. H. & Li, X. J.
Chaperone suppression of cellular toxicity of huntingtin is independent of polyglutamine aggr egation. J Biol Chem. 276, 48417-24 (2001)

Muchowski, P. J., Schaffar, G., Sittler, A., Wanker, E. E., Hayer-Hartl, M. K. & Hartl, F. U. Hsp70 and hsp40 chaperones can inhibit self-
assembly of polyglutamine proteins into amyloid-like fibrils. Proc Natl Acad Sci U S A. 97, 7841-6 (2000)

Wyttenbach, A., Carmichael, J., Swartz, J., Furlong, R. A., Narain, Y., Rankin, J. & Rubinsztein, D. C. Effects of heat shock, heat shock protein 40 (HDJ-2),
and proteasome inhibition on protein aggregation in cellularmodels of Huntington's disease. Proc Natl Acad Sci U S A. 97, 2898-903 (2000)

Chai, Y., Koppenhafer, S. L., Bonini, N. M. & Paulson, H. L. Analysis of the role of heat shock protein (Hsp) molecular chaperones in polyglutamine disease. J Neurosci. 19, 10338-47 (1999).

Summary in Korean

요 약 문

폴리글루타민 단백질과 글루타민을 많이 포함하는 표적 단백질 간의 상호작용의 특성 분석

폴리글루타민 질병 (Polyglutamine disease)과 같이 단백질 독성에 의해 발병되는 많은 뇌 질환들의 병리기전을 이해하기 위해서는 이러한 독성을 띄는 단백질들이 어떻게 다른 많은 단백질들과 상호작용하고 붙잡는지 이해하는 것이 매우 중요하다. 하지만 특히 홀리글루타민 질병에서는 독성 단백질과 다른 단백질 간에 상호작용 (interaction)하기 위해 요구되는 특성에 대해서 거의 알려진 것이 없다. 이 연구에서 우리는 폴리글루타민 단백질과 그들의 표적이 될 수 있는 단백질 (target proteins)들 간의 상호작용에서 필요한 특성이 무엇인지 관찰하고, 표적이 되는 단백질들이 폴리글루타민 단백질의 응집체 형성 (aggregate formation)에 어떤 영향을 미칠 수 있는지 알아보았다. 우리는 글루타민 아미노산들이 (Q-Q) 서로 상호작용을 일으킬 것으로 예상하여 병원성 폴리글루타민 단백질과 글루타민 (Q)을 많이 포함하는 표적 가능성이 있는 단백질들이 신경세포 안에서 상호작용 하는 것을 확인했다. 더 나아가, 우리는 새로운 전략으로써 구조적 억제자

(structural inhibitor)를 사용해 병원성 폴리글루타민 단백질과 다른 표적 단백질의 상호작용을 조절 할 수 있는지 확인해 보았다. 종합하면, 이러한 연구를 통하여 우리는 병원성 폴리글루타민 단백질과 글루타민을 많이 가지고 있는 표적 가능성이 있는 단백질간의 상호작용의 형태/유형을 연구 할 수 있는 독자적인 모델 시스템을 구축하고, 폴리글루타민 단백질과 표적 가능성이 있는 단백질 간의 상호작용에서 표적 단백질이 접착제 (glue)와 같은 기능으로 작용하여 병원성 폴리글루타민 질환의 단백질 응집체 형성을 가속 화 시킬 수 있다는 가능성을 제시하였다.

핵심어 : 폴리글루타민 질병, 글루타민을 많이 갖는 단백질, 표적 단백질, 상호작용, 접착제 작용 이론